Journal of Computational Physics 228 (2009) 4881–4892

Contents lists available at ScienceDirect

Journal of Computational Physics

journal homepage: www.elsevier.com/locate/jcp

Understanding the accuracy of Nanbu's numerical Coulomb collision operator

Andris M. Dimits [a,*], Chiaming Wang [b], Russel Caflisch [b], Bruce I. Cohen [a], Yanghong Huang [b]

[a] Lawrence Livermore National Laboratory, Fusion Energy Program, P.O. Box 808, Livermore, CA 94550, USA
[b] Mathematics Department, University of California at Los Angeles, Los Angeles, CA 90036, USA

ARTICLE INFO

Article history:
Received 10 August 2008
Received in revised form 23 February 2009
Accepted 30 March 2009
Available online 10 April 2009

Keywords:
Coulomb collisions
Lorentz collisions
Numerical methods
Monte Carlo methods
Collisional plasma

ABSTRACT

We investigate the accuracy of and assumptions underlying the numerical binary Monte Carlo collision operator due to Nanbu [K. Nanbu, Phys. Rev. E 55 (1997) 4642]. The numerical experiments that resulted in the parameterization of the collision kernel used in Nanbu's operator are argued to be an approximate realization of the Coulomb–Lorentz pitch-angle scattering process, for which an analytical solution for the collision kernel is available. It is demonstrated empirically that Nanbu's collision operator quite accurately recovers the effects of Coulomb–Lorentz pitch-angle collisions, or processes that approximate these (such interspecies Coulomb collisions with very small mass ratio) even for very large values of the collisional time step. An investigation of the analytical solution shows that Nanbu's parameterized kernel is highly accurate for small values of the normalized collision time step, but loses some of its accuracy for larger values of the time step. Careful numerical and analytical investigations are presented, which show that the time dependence of the relaxation of a temperature anisotropy by Coulomb–Lorentz collisions has a richer structure than previously thought, and is not accurately represented by an exponential decay with a single decay rate. Finally, a practical collision algorithm is proposed that for small-mass-ratio interspecies Coulomb collisions improves on the accuracy of Nanbu's algorithm.

1. Introduction

Modeling of Coulomb interactions is important to the understanding of many plasma systems. For an inter-particle distance d larger than the Debye length λ_D, Coulomb interactions are mediated through electro-magnetic fields governed by the Vlasov equation. On the other hand, if $d < \lambda_D$, these interactions can be described as Coulomb collisions, governed by the Fokker–Planck equation. There is a long history of study of Coulomb collisions in plasmas. The 1965 review paper by Trubnikov [1] contains many of the important analytical results for relaxation processes associated with Coulomb collisions.

This paper considers issues important to Monte Carlo particle methods for simulation of Coulomb collisions. One of the earliest and most influential Monte Carlo collision algorithms was a binary algorithm developed by Takizuka and Abe (TA) [2]. In this model, the particles are paired locally in space and undergo binary elastic scattering events, which conserve particle number, energy, and momentum. Viewed in the center-of-mass frame of a binary scattering pair, the relative velocity, the magnitude of which is preserved, scatters through some angle $\Delta\theta$. The distribution of the angles $\Delta\theta$ is chosen so that for a short time step Δt such that $\nu\Delta t \ll 1$, where ν is a mean collision rate, $\Delta\theta$ is small; and the accumulation of many collision events gives an evolution in agreement with the Landau–Fokker–Planck operator for Coulomb collisions. This scheme was modified by Nanbu [3]. Nanbu aimed to develop a scheme in which the collisions were aggregated so that a single large time

* Corresponding author. Tel.: +1 925 422 0211; fax: +1 925 423 3484.
E-mail address: dimits1@llnl.gov (A.M. Dimits).

0021-9991/$ - see front matter © 2009 Elsevier Inc. All rights reserved.
doi:10.1016/j.jcp.2009.03.041

step (i.e., $\nu\Delta t$ not necessarily small) would still yield an evolution (for example, of the distribution of collision angles) that accurately represents an accumulation of Coulomb collisions. The two methods proposed by TA and Nanbu have been widely used in the plasma physics community [4–9]. The questions addressed in this paper are the following: (1) What is the physics basis for Nanbu's collision kernel [3]? (2) how accurate is Nanbu's collision kernel and numerical collision operator over a range of time-step and mass-ratio values?

Wang et al. [10] performed a numerical convergence study for the methods of TA and Nanbu, and the latter method formed the basis for a hybrid simulation scheme developed by Caflisch et al. [11]. In [10], it was found that both for ion–ion and electron–ion collisions, the pointwise errors for the Nanbu method were comparable to those of the TA method run at approximately half the timestep. Thus the collision aggregation was at best partially successful.

In the remainder of this paper, we further study the accuracy of and assumptions underlying Nanbu's collision operator [3]. In Section 2, it is argued that collision kernel in [3] is an empirically obtained parameterization of the kernel for the Coulomb–Lorentz pitch-angle scattering (diffusion) process, for which an analytical expression is known [1]. It is also demonstrated empirically there that Nanbu's collision operator quite accurately recovers the effects of such collisions, even for very large values of the collisional time step. In Section 3, the analytical Coulomb–Lorentz and Nanbu kernels are evaluated and compared. It is shown that the latter is a highly accurate approximation for small values of the normalized collision time step, but loses some of its accuracy for larger values of the time step.

The primary motivation for studies reported here is to understand the regimes, in numerical parameter space, of validity of Nanbu's operator. Nanbu's operator is accurate for sufficiently short time steps (and sufficiently large particle number). For the widely considered temperature-anisotropy-relaxation test problem [1–3,10,12], we are able to delineate the regime of validity. The breakdown of accuracy of Nanbu's operator as a function of time step and mass ratio occurs because energy diffusion competes with isotropization (i.e., diffusion in pitch angle). This energy diffusion can be thought of as a surrogate for other processes that may compete with isotropization in more complicated plasma systems. Thus, the temperature-anisotropy relaxation problem gives, at least at a qualitative level, information about the breakdown in accuracy of the Nanbu (and any Lorentz-kernel based) operator in more realistic situations.

A secondary motivation for our study of the accuracy of Nanbu's kernel as a parameterization of the (Lorentz) collisions of the numerical experiments in Ref. [3] is interest in the Coulomb–Lorentz operator itself. The "Lorentz-gas model" has been widely discussed as a pedagogical model and a reasonable approximation that qualitatively captures the important effects of collisions in gas-dynamic [13] and plasma [14] systems. A Coulomb–Lorentz-based kernel, and Nanbu's operator (or a more accurate version) may also be useful for the quantitative modeling of parts of some plasma systems when time scale separation is present. An example is the slowing down of fast electrons by a high-Z plasma (where Z is the ion charge) as occurs, for example, in fast-ignition inertial-confinement-fusion targets [15]. Because of the Z dependence of the Coulomb collision rates, the collisions of the fast electrons with the target ions dominate over collisions with the target electrons. Although a key quantity of interest is the energy loss of the fast electrons, which results primarily through collisions with the target electrons, this process occurs on a significantly slower time scale than the electron–ion collisional isotropization. Thus, a Lorentz-kernel based operator, such as that of Nanbu or the modification outlined in Section 5, may be useful to represent the isotropization process, as it will allow time steps of the order of the electron–ion collision time.

In Section 4, the relaxation of a temperature anisotropy by Coulomb–Lorentz collisions is examined in more detail, using the analytical kernel from [1]. Based on the results of Section 3, a practical collision algorithm is proposed in Section 5, which for small-mass-ratio interspecies Coulomb collisions improves on the accuracy of Nanbu's algorithm. Conclusions of this study are given in Section 6.

2. Accuracy of the Nanbu operator for long time steps

Some insight into the accuracy and applicability of the Nanbu operator can be gained by realizing that the collision kernel given by Nanbu is actually derived from numerical experiments in which the orientation vector (only) of the velocity of a test particle evolves. This evolution does not take into account the interaction between different pairs of particles, which would result in evolution of the energy of the distribution (or of a test particle). Furthermore, in the numerical experiment of Nanbu this orientation undergoes repeated small deflections (a typical value of the variance being $\langle(\Delta\theta)^2\rangle \approx 3\times 10^{-3}$), each of which is independent of the orientation itself and of the previous deflections. Such a process is well described by the Lorentz collision operator, which represents diffusion with a uniform (i.e., independent of orientation) diffusion coefficient on a (unit) sphere of the tips of the orientation vectors.

$$\frac{\partial f_a}{\partial s} = \frac{\partial}{\partial \mu}\left[(1-\mu^2)\frac{\partial f_a}{\partial \mu}\right] + \frac{1}{(1-\mu^2)}\frac{\partial^2 f_a}{\partial \phi^2}, \tag{2.1}$$

where $\mu = \cos\theta$, θ is the polar angle with respect to some point designated as the pole on the sphere, and ϕ is the azimuthal angle. The normalized time parameter $s = t/2\tau_s^{\alpha/\beta}$, where t is the physical time, and $\tau_s^{\alpha/\beta}$ is the longitudinal slowing down time [1] for a charged particle of species α colliding off a particle of species β:

$$\tau_s^{\alpha/\beta} = \frac{v^3}{4\pi\Lambda^{\alpha/\beta} n_\beta}\left(\frac{m_\alpha}{q_\alpha q_\beta}\right)^2.$$

Here, v is the test particle's speed, $\Lambda^{\alpha/\beta}$ is the "Coulomb logarithm" [1], and n_α, m_α, and q_α are respectively the number density, mass, and charge of a particle of species α. The operator in Eq. (2.1) and the analytical solution for its kernel (which is the solution from a point initial condition at $\theta = 0$) have long been known [1]. The association between the numerical experiments of Nanbu [3] and Lorentz collisions, as well as the analytical solution for the (kernel of the) latter were also noted by Bobylev and Nanbu [16]. The numerical evaluation of this analytical solution is straightforward, and is carried out in Section 3. A comparison of Nanbu's parameterization with this solution, also given there, shows that Nanbu's parameterization is an excellent approximation for short time steps, and a quite good approximation for all values, with a maximum relative error of about 8%.

It follows from the above arguments that for Coulomb collisions of charged particles off much heavier (e.g., electrons colliding off ions) or infinitely heavy scatterers, Nanbu's collision operator should be accurate even if very large time steps are used. This indeed appears to be the case. Fig. 1 shows the results for the collisional isotropization test of [10], using the Nanbu collision operator, in the limit of zero mass ratio. In this test, the particles are loaded as an anisotropic Maxwellian with different parallel and perpendicular temperatures. The initial relative temperature anisotropy is $\Delta T/T = 0.15$, where $\Delta T \equiv T_\parallel - T_\perp$ and $T = (T_\parallel + 2T_\perp)/3$. These runs use 1.6×10^5 particles. The curves in Fig. 1 are the time histories of the temperature isotropy, normalized to their initial values, for simulations that used the four different time step values $\nu_0\Delta t = 0.22$, 1.1, 2.2, and 3.3, and for the analytical result [1,12,17]:

$$\frac{\Delta T(t)}{\Delta T(0)} = \exp\left(-\frac{2}{5\sqrt{\pi}}\nu_0 t\right). \tag{2.2}$$

Here ν_0 is a thermally averaged collisional relaxation rate, given by

$$\nu_0 = \frac{1}{\tau_s^{e/\beta}(v = v_{\text{the}})} = \frac{4\pi\Lambda^{e/\beta} n_\beta e^2 q_\beta^2}{\sqrt{m_e} T_e^{3/2}},$$

$v_{\text{the}} = \sqrt{T_e/m_e}$ is the electron thermal velocity, and $e = q_e$ is the absolute value of the electron charge. It is seen that the relaxation process is well represented even when the very long time steps $\nu_0\Delta t = 1.1$–3.3 are used. At late times ($\nu_0 t \geq 4$), the simulation curves systematically depart from the analytical curve. The reason for this departure, which will be further examined in Section 3, is that the Eq. (2.2) is valid only for short times.

Fig. 2 shows results for the collisional isotropization test, now with mass ratio $m_e/m_i = 10^{-4}$, for two different ensembles of 10 realizations, each with 8×10^3 electrons and the same number of ions, for several values of the time step. The two ensembles use different realizations of the initial loading and of the random numbers used in the collisions. Again, as for all of the simulation results shown in this section, with the exception of the TA curves in Fig. 4, the Nanbu collision operator is used. In the first ensemble [Fig. 2(a)], for all but the two shortest time step cases, there is a departure of the temperature difference from the analytical result after the first time step. This departure subsequently decays. Apart from this, the temperature difference curves are similar for the two ensembles. Additional simulations show that the early departure of the simulation results is quite prevalent, and the degree of departure from the analytical curve is a more strongly a function of the particular realization of the initial particle loading (i.e., velocity values), than of the particular realizations of the random number sets used in the collision operator.

Fig. 3 shows results from a time step scan using ensemble averages over sets of 80 runs with different initial-condition and collision random number seeds. Here again, the mass ratio is $m_e/m_i = 10^{-4}$, and the other numerical parameters are as for the runs in Fig. 2, with the exception that the time step choices are not identical. This figure indicates that the departure of the long time step curves from the shorter time step cases during the first one or two time steps occurs in a significant

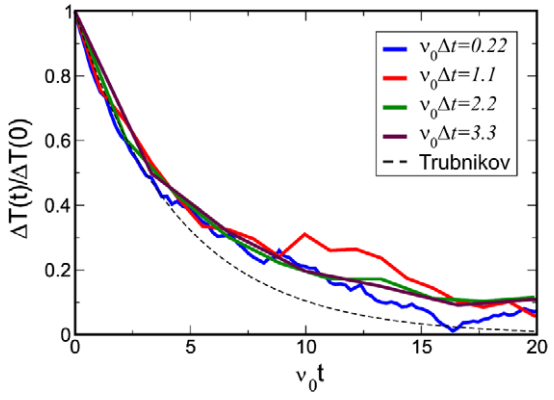

Fig. 1. Results for the collisional isotropization test of [10] for Lorentz collisions (zero mass ratio m_e/m_i), for four different values of the time step. Also shown is the analytical result from [17].

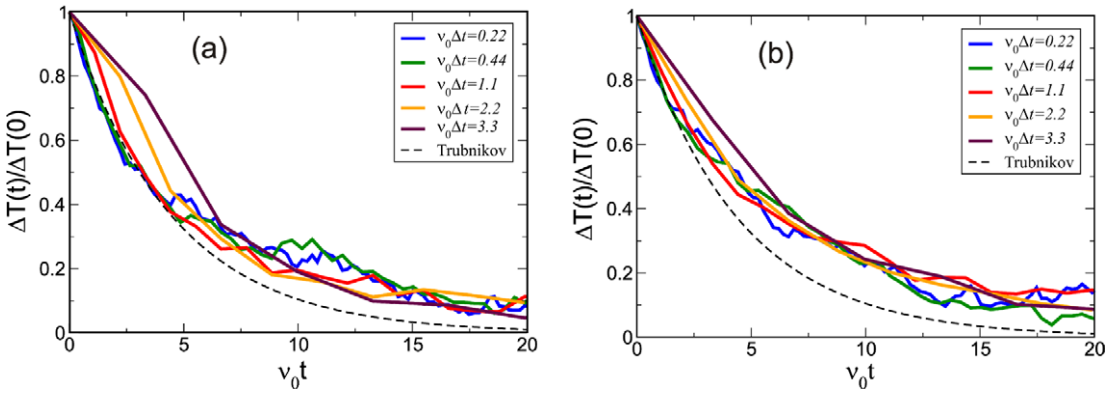

Fig. 2. Results for the collisional isotropization test for mass ratio $m_e/m_i = 10^{-4}$, for two ensembles, for $\nu_0\Delta t = 0.22$, 0.44, 1.1, 2.2 and 3.3.

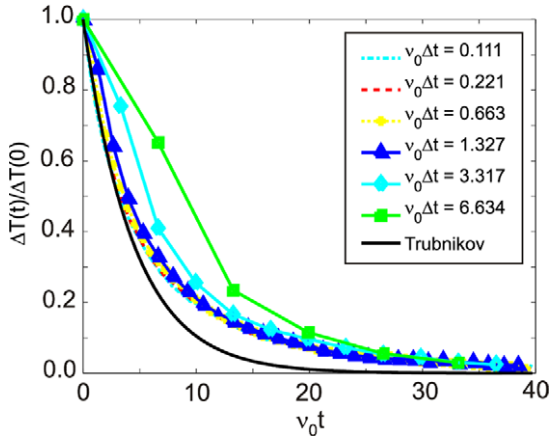

Fig. 3. Results for the collisional isotropization test for mass ratios $m_e/m_i = 10^{-4}$, averaged over 80 realizations of the initial loading, for $\nu_0\Delta t$ ranging from 0.11 to 6.6.

fraction of the realizations in the ensembles. Again, as for Fig. 1, the curves in Figs. 2 and 3 show departures from the analytical formula, which over predicts the relaxation at intermediate and late times.

Fig. 4 shows a comparison of the Nanbu and TA operators for the collisional isotropization test for two ensembles with the same realizations of the electron loading as for those in Fig. 2, with $\nu_0\Delta t = 1.1$, and with other numerical parameters as in Fig. 2. This shows that the TA operator is much less accurate than the Nanbu operator for large timesteps and small mass ratio.

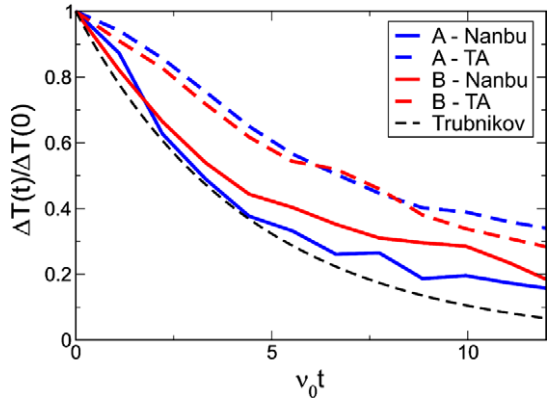

Fig. 4. Comparison of the TA and Nanbu operators for the collisional isotropization test for $m_e/m_i = 10^{-4}$, and $\nu_0\Delta t = 1.1$. Cases *A* and *B* correspond to the initial loading used in Fig. 2(a) and (b), respectively.

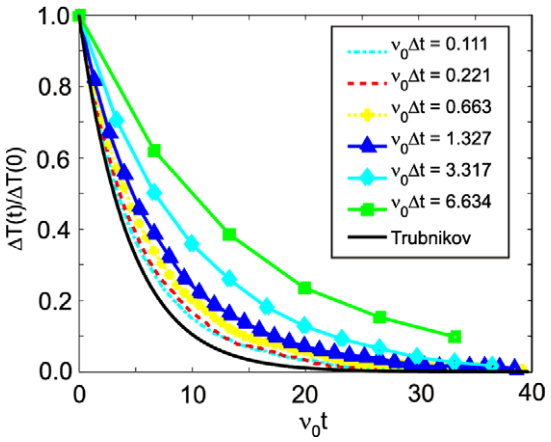

Fig. 5. Results for the collisional isotropization test for $m_e/m_i = 1$, averaged over 80 realizations of the initial loading, for $\nu_0\Delta t$ ranging from 0.11 to 6.6.

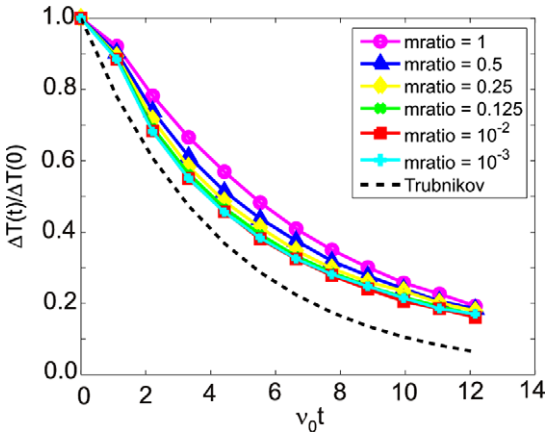

Fig. 6. Results for the collisional isotropization test for mass ratios m_e/m_i ranging from 10^{-3} to 1, for the same two realizations of the initial loading as in Fig. 2, with $\nu_0\Delta t = 1.1$.

Fig. 5 shows the results for a time-step scan for the collisional isotropization test, now with $m_e/m_i = 1$, and with ensemble averaging as in Fig. 3. The electron and ion charges used are also the same, so these cases can also be considered as like-particle (e.g., electron–electron or ion–ion) scattering cases. For small values of time step, there is good agreement between the simulation and analytical results. As the time step increases, the level of agreement degrades, with a systematically increasing underprediction of the relaxation. This is to be expected [1], since energy evolution is important for $m_e/m_i = 1$, and the relaxation process is no longer accurately represented by Lorentz pitch-angle scattering alone. This loss of accuracy was not present in the small and zero mass-ratio cases.

Fig. 6 shows the results for a range of mass ratios ($m_e/m_i = 1$, 0.5, 0.25, 0.125, 10^{-2}, 10^{-3}) in the collisional isotropization test using $\nu_0\Delta t = 1.1$, averaged over 80 realizations of the loading. It is seen that the agreement is best for very small values of the mass ratio, and degrades as the mass ratio increases. This degradation is again a sign of the increasing importance of processes other than pitch-angle scattering (e.g., energy evolution in the present case) as the mass ratio increases from 0 to 1.

3. Analytical solution for the Coulomb–Lorentz collision kernel, and comparison with Nanbu's parameterization

As argued in the previous section and in [16], the numerical experiments upon which Nanbu's kernel is based are actually numerical realizations of the Coulomb–Lorentz collision process, which is described by Eq. (2.1), and for which the analytical solution has been obtained (for example, in [1]). This solution is

$$f_a(\theta,t) = f(\mu,s) = \frac{1}{2\pi}\sum_{l=0}^{\infty}\left(l+\frac{1}{2}\right)P_l(\mu)\exp[-l(l+1)s]. \tag{3.1}$$

(Recall that μ=cosθ.) The normalization, which is set by the initial condition, is chosen so that

$$2\pi \int_{-1}^{1} d\mu f(\mu, s) = 1. \tag{3.2}$$

Note also that the identification of Nanbu's normalized time parameter $s = \langle\theta_1^2\rangle N/2$ with the time normalized to Trubnikov's collision time scale τ_s time, $s = t/(2\tau_s)$ is easily made. Nanbu's parameterization [3] of this solution is obtained empirically from a simulation study. He notes that the solutions are quite accurately represented by linear approximations to the dependence of log[$f(\mu)$] on μ. Furthermore, by empirical examination and analysis of the short-time (small-s) dependence, he finds

$$\langle \sin^2\theta/2\rangle = \frac{1}{2}(1 - \langle\mu\rangle) = \frac{1}{2}(1 - e^{-s}). \tag{3.3}$$

This can be recovered easily from Eq. (3.1). From Eqs. (3.2) and (3.3), and the assumption of a linear dependence of log[$f(\mu)$] on $\mu = \cos\theta$, it follows that

$$N(\mu, s) = \frac{A(s)}{4\pi \sinh A(s)} \exp[A(s)\mu], \tag{3.4}$$

where A satisfies

$$\coth A(s) - 1/A(s) = e^{-s} \tag{3.5}$$

In order to enable detailed comparisons, we have coded both Eq. (3.1) and Nanbu's parameterization, Eqs. (3.4) and (3.5), in Mathematica.

We can assess the accuracy of the analytical curves by comparing the results with different numbers of terms retained. Fig. 7 shows such a comparison, plotting log(f) as a function of μ. It is seen that 8 terms are sufficient for good accuracy of any integrals involving $f(\mu)$ for $s = 0.2$ or larger. Note that for $s = 0.2$, the departure between the 8- and 14-term result occurs when $f(\mu)$ is a factor of $e^{-10} \cong 5 \times 10^{-5}$ below its maximum value. The places where the logarithm curves take very large negative values represent oscillations through zero.

We now examine the time evolution of using enough terms to ensure good accuracy.

Fig. 8 shows the dependence of log(f), as given by Eq. (3.1) on μ at the times (s values) corresponding to those of Fig. 2 in [3]. These curves agree very well with those in [3]. Here, the values of s were obtained using, $s = \langle\theta_1^2\rangle N/2$ with N as given in Fig. 2 of [3], and $\langle\theta_1^2\rangle = 3.0524 \times 10^{-3}$, which is the value used by Nanbu in that figure.

The direct evaluation of Eq. (3.1), shown in Fig. 8, is a more accurate solution to the Lorentz collisional evolution than the parameterization of [3], provided that enough terms are kept in the sum in Eq. (3.1). At low values of f, Nanbu's empirical

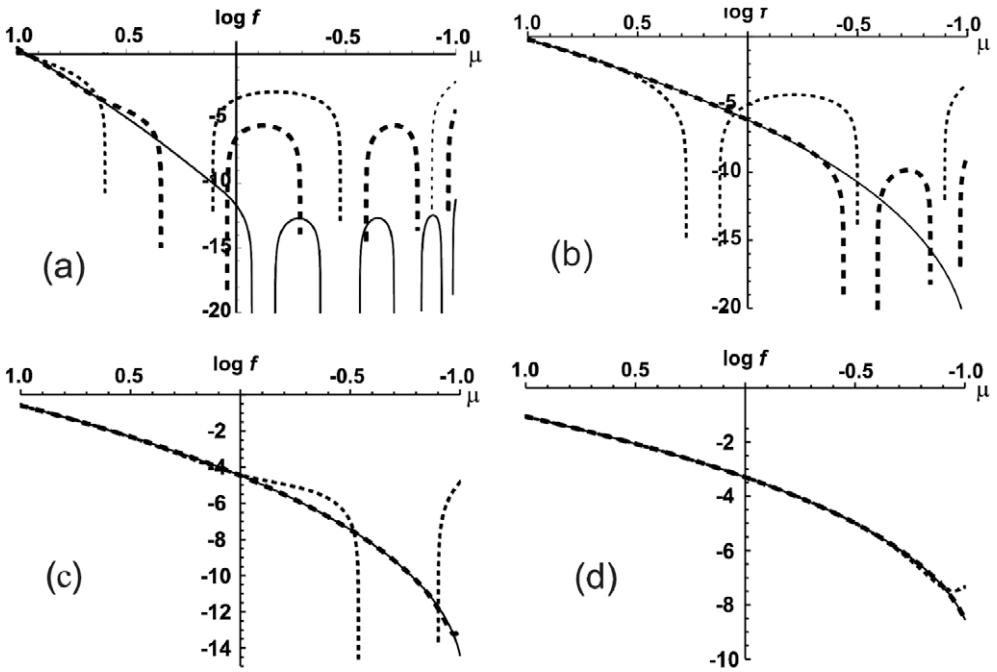

Fig. 7. Comparison of log$f(\mu)$, where $\mu = \cos\theta$ from Eq. (3.1) using 4 terms (small dashed), 8 terms (thick dashed), and 14 terms (solid) for (a) $s = 0.1$, (b) $s = 0.2$, (c) $s = 0.3$, and (d) $s = 0.5$.

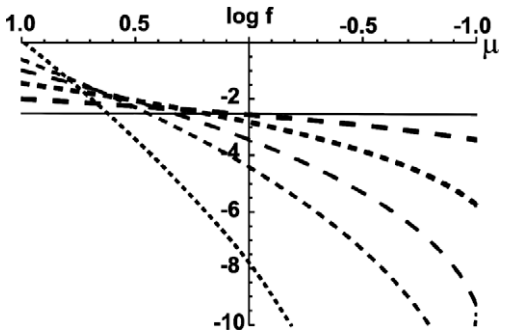

Fig. 8. Evolution of f from Eq. (3.1) at times (s = 0.153, 0.305, 0.458, 0.763, 1.53, 4.58) corresponding to those of Fig. 2 in [3]. The curves can be identified with their s values by noting that for larger s, the curves become less steep.

results are affected by noise. This explains the fact that the curves in Fig. 2 of [3] trend up from the linear fits at small values of s, while the curves resulting from the analytical solution trend down.

For a more detailed comparison, we have solved Eq. (3.5) for $A(s)$, and inserted the result into Eq. (3.4). A comparison between the results of Eqs. (3.4) and (3.5) vs. Eq. (3.1) for s = 0.1, 0.2, and 0.3 is shown in Fig. 9. The curves from Eq. (3.1) were made using 32 terms in the sum for the s = 0.1 curve, and 16 terms for the s = 0.2 and 0.3 curves.

It is seen that for small values of s, Nanbu's parameterization gives an excellent approximation to the analytical result, and that the quality of the fit degrades as time increases.

The excellent fit at early times can be understood from the fact that the process represented by Eq. (2.1) is diffusion on a unit sphere with a constant and uniform diffusion coefficient. The particular solution given by Eq. (3.1) is for the evolution from an initial condition that is proportional to a delta function at the pole, i.e.,

$$f_a(\theta,t) = \frac{1}{2\pi}\delta(1-\mu).$$

For short times, such that the solution is sufficiently localized to not sense the curvature of the sphere (i.e., $\mu \cong 1, \theta \cong 0$), Eq. (2.1) becomes

$$\frac{\partial f_a}{\partial s} \simeq \frac{1}{\theta}\frac{\partial}{\partial \theta}\left[\theta \frac{\partial f_a}{\partial \theta}\right], \tag{3.6}$$

where the axial symmetry of the initial condition and resulting solution has also been used. Eq. (3.6) is recognized as the equation for diffusion on a plane with axial ("cylindrical") symmetry and uniform diffusion coefficient. The solution of Eq. (3.6), consistent with Eq. (3.2) is

$$f_a(\theta,t) = \frac{1}{2\pi s}\exp\left(-\frac{\theta^2}{2s}\right) \quad \forall s > 0. \tag{3.7}$$

Examining Eqs. (3.4) and (3.5) for small s, we see that the solution of Eq. (3.5) for small s (and large A) is $A \cong s^{-1}$. Upon inserting this into Eq. (3.4), we recover Eq. (3.7).

We now examine the accuracy of Nanbu's parameterization for larger s. A comparison between the results of Eqs. (3.4) and (3.5) vs. Eq. (3.1) for s = 0.5, 1.0, and 2.0 is shown in Fig. 10.

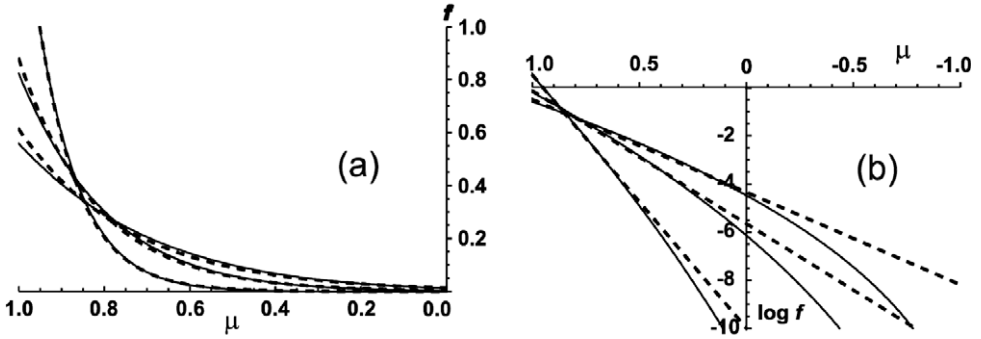

Fig. 9. Comparison for (a) f and (b) log(f), between the results of Eqs. (3.4) and (3.5) (dashed curves) and Eq. (3.1) (solid curves) for s = 0.1, 0.2, and 0.3. The curves can be identified with their s values by noting that for larger s, the curves become less steep.

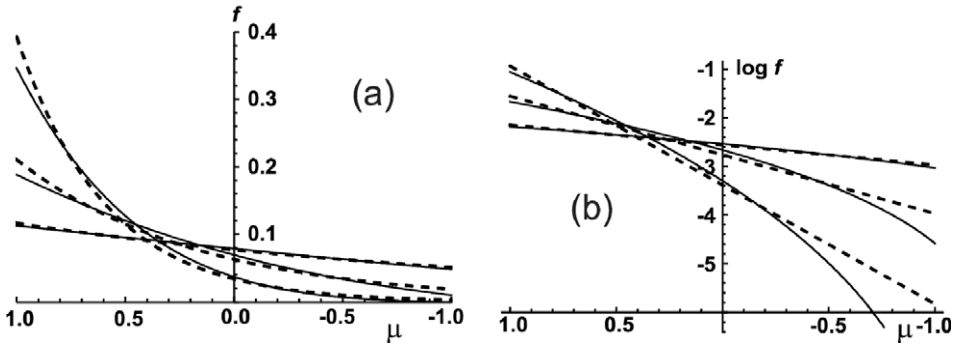

Fig. 10. Comparison for (a) f and (b) $\log(f)$, between the results of Eqs. (3.4) and (3.5) (dashed curves) and Eq. (3.1) (solid curves) for $s = 0.5$, 1.0, and 2.0. Again, the curves can be identified with their s values by noting that for larger s, the curves become less steep.

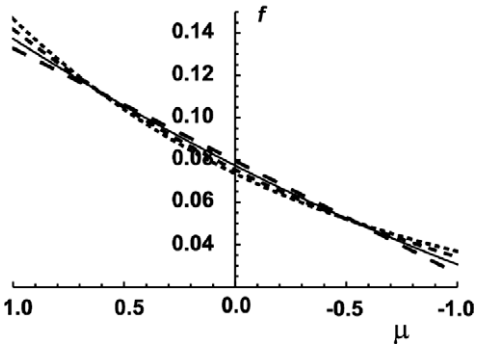

Fig. 11. Comparison between the results of Nanbu's Kernel (Eqs. (3.4) and (3.5) – small dashed curve), Eq. (3.1) with 2 terms kept in the sum (long-dashed curve), Eq. (3.1) with 16 terms kept in the sum (solid curve), all for $s = 1.5$, and a convolution of two Nanbu Kernels Eqs. (B.1) and (B.2), each with $s = 0.75$ (medium dashed curve).

For these larger values of s, Nanbu's parameterization gives a reasonably good approximation to the analytical result, but is not nearly as accurate as for the smaller s values. The departure can be understood from the fact that at large s, the exponential formula of Eq. (3.4) intrinsically has more curvature than the true solution, which is quite accurately approximated by the first two (linear in μ.) terms Eq. (3.1). Fig. 11 shows a comparison between the accurate result, Eq. (3.1) with many terms kept, Eq. (3.1) with 2 terms kept, and Nanbu's formula at $s = 1.5$. It is seen that the 2-term result, which keeps only the uniform ($P_0(\mu) = 1$) and linear ($P_1(\mu) = \mu$) terms, is a quite accurate approximation. In contrast, the curve from Eq. (3.4) has significantly more curvature than the true solution. Also, it is seen that Eq. (3.4) slightly overestimates the value of the kernel near $\mu \cong \pm 1$, and slightly underestimates it near $\mu = 0$. A predictable consequence of this difference is that for values of $s \cong 1$–2, the application of an operator based on this formula to isotropization by Lorentz collisions will slightly underpredict isotropization rates (e.g., in the temperature isotropization tests in the previous section) in the first time step, such as that seen in Figs. 2–4 and 6. The result of two applications of Nanbu's Kernel, which is calculated in Appendix B, with times (s values) s_1, and s_2 such that $s_1 + s_2 = s$ is a better approximation to the analytical kernel than a single application of Nanbu's Kernel with time s. An example of this is also shown in Fig. 11.

4. Analytical solution for the relaxation of temperature anisotropy by Coulomb–Lorentz collisions

The problem of relaxation of a small temperature anisotropy by like-particle Coulomb collisions was studied by Kogan [12,1]. An approximate parameterization, extending this result to Coulomb collisions of test particles with field particles of different mass as well as to large values of the temperature difference, is given in [17]. The results of [12] and the small temperature anisotropy limit of the result in [17] both predict an exponential temperature decay as given by Eq. (2.2). It is seen, for example in Figs. 1 and 3, that Eq. (2.2) does not predict the temperature anisotropy decay well for $\nu_0 t \gtrsim 4$. This discrepancy motivates a more detailed examination of the relaxation. For the case of small mass ratio (Lorentz scattering), this examination is greatly facilitated by the analytical result of Eq. (3.1), which allows for a closed-form expression for the evolution valid for all times.

The temperature anisotropy can be written as

$$\Delta T = T_\perp - T_\parallel = m(\langle v_\perp^2/2\rangle - \langle v_\parallel^2\rangle) = -m\langle v^2 P_2(\mu)\rangle, \tag{4.1}$$

where $\langle\psi(v,\mu)\rangle$ represents and integral of ψ (v,μ) over the distribution function.

For an initial state with Maxwellian distributions in the parallel and transverse directions, the use of a small anisotropy approximation results in a simple and useful form for the distribution function:

$$f(v,\mu,t=0) = F_m(v) + \delta f(v,\mu,t=0),$$

where

$$F_m(v) = \frac{1}{\left(\sqrt{2\pi}v_{th}\right)^3}\exp\left(-\frac{v^2}{2v_{th}^2}\right)$$

is the equilibrium Maxwellian, and

$$\delta f(v,\mu,t=0) = \frac{1}{3v_{th}^2}\frac{\Delta T}{T}\left(\frac{1}{2}v_\perp^2 - v_\parallel^2\right)F_m(v) = -\frac{1}{3v_{th}^2}\frac{\Delta T}{T}v^2P_2(\mu)F_m(v).$$

Here, $v_{th}^2 = T/m$, T is the equilibrium temperature, and m is the particle mass. By applying the kernel of Eq. (3.1), or by simply noting that under Lorentz collisions, the $P_2(\mu)$ component decays as $\exp[-3t/\tau_s(v)] = \exp(-3tv_{th}^3/[v^3\tau_s(v_{th})])$, we obtain

$$\delta f(v,\mu) = -\frac{1}{3}\frac{\Delta T}{T}\frac{v^2}{v_{th}^2}P_2(\mu)F_m(v)\exp\left[-3\frac{v_{th}^3}{v^3}\frac{t}{\tau_s(v_{th})}\right]. \tag{4.2}$$

Inserting Eq. (4.2) into Eq. (4.1) and integrating over μ yields

$$\Delta\widehat{T}(t) \equiv \frac{\Delta T(t)}{\Delta T(0)} = \sqrt{\frac{2}{\pi}}\frac{1}{15v_{th}^7}\int_0^\infty dv v^6\exp\left[-\frac{1}{2}\left(\frac{v^2}{v_{th}^2} + \frac{6v_{th}^3}{v^3}\frac{t}{\tau_s(v_{th})}\right)\right]. \tag{4.3}$$

It can easily be verified that

$$\Delta\widehat{T}(0) \equiv \sqrt{\frac{2}{\pi}}\frac{1}{15v_{th}^7}\int_0^\infty dv v^6\exp\left[-\frac{v^2}{2v_{th}^2}\right] = 1.$$

For small t/τ_s, Eq. (4.3) gives

$$\Delta\widehat{T}'(0) \equiv \frac{d\Delta\widehat{T}(t)}{dt}|_{t=0} = -\frac{1}{\tau_s(v_{th})}\sqrt{\frac{2}{\pi}}\frac{1}{5v_{th}^4}\int_0^\infty dv v^3\exp\left(-\frac{v^2}{2v_{th}^2}\right) = -\frac{2}{5}\sqrt{\frac{2}{\pi}}[\tau_s(v_{th})]^{-1}. \tag{4.4}$$

Somewhat paradoxically, the early-time decay rate predicted by Eq. (4.4) is a factor of $\sqrt{2}$ greater than that of Eq. (2.2). The quality of various approximations can be better understood by comparing them with the result of direct numerical evaluation of Eq. (4.3). [We have also examined approximate saddle-point evaluations of Eq. (4.3) but have found that these give little additional insight because either a numerical evaluation of the saddle point location and other related parameters is needed or else the quality of the resulting approximation is poor.] The results of such a comparison, between the result of Eq. (4.3) and exponential decay with decay rates given by Eqs. (2.2) and (4.4), are shown in Fig. 12. It is seen that although the decay with rate given by Eq. (4.4) is an accurate approximation for very early times ($\nu_0 t \le 0.3$), for $\nu_0 t > 1$ the exponential decay with rate given by Eq. (2.2) is a much more accurate representation of Eq. (4.3). The departure of the exponential decay with rate given by Eq. (2.2), from Eq. (4.3) for $\nu_0 t > 4$, as well as the value $\Delta\widehat{T}(\nu_0 t = 20) = 0.076$ are both in agreement with the numerical results shown in Figs. 1 and 3.

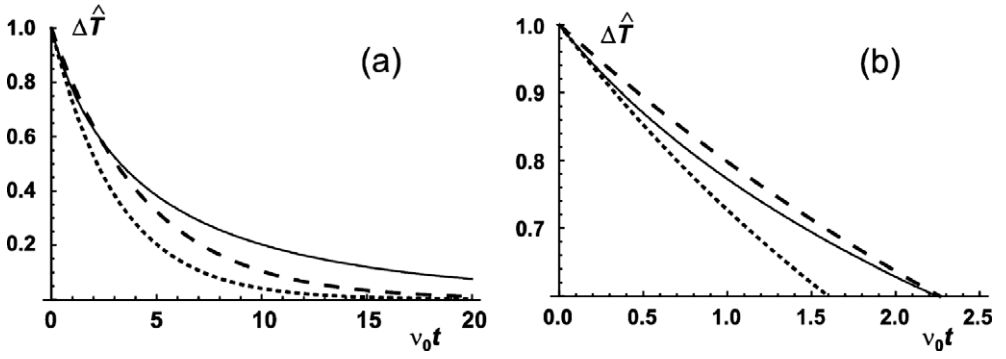

Fig. 12. Comparison of the temperature anisotropy decay vs. time as predicted by Eq. (4.3) (solid curve) with exponential decay with rates given by Eq. (2.2) (large-dashed curve) and Eq. (4.4) (small dashed curve), on two different scales. (Frame (b) shows detail of the early-time dependence.)

5. Improvement of Nanbu's collision operator for Coulomb–Lorentz collisions

An improvement to Nanbu's operator, at least for application to Lorentz (small-mass-ratio) collisions can be made based on Eq. (3.1) and the insight gained in the studies in the previous section. We outline this improvement here, but leave implementation for future work.

It follows from the results of the previous section that an accurate approximation to the kernel for the Lorentz collision operator can be obtained by using a matched expression in which Nanbu's form [Eqs. (3.4) and (3.5)] is used for $s \leq s_0$, and Eq. (3.1) with a finite number of terms is used for $s > s_0$. While further optimization is possible, the results shown in Figs. 7 and 9 indicate that an accurate combination is given by $s_0 = 0.1$, and 14 terms in the sum in Eq. (3.1). In addition, for $s_0 > 4.0$, two terms in Eq. (3.1) give an accurate approximation, and the leading ($l = 0$, independent of μ) term is strongly dominant. Thus, a good approximation is:

$$f_a(\mu,s) = \begin{cases} \frac{A(s)}{4\pi \sinh A(s)} \exp[A(s)\mu], & \text{for} \quad s \leqslant 0.1, \\ \frac{1}{2\pi}\sum_{l=0}^{13}\left(l+\frac{1}{2}\right)P_l(\mu)\exp[-l(l+1)s], & \text{for} \quad 0.1 < s \leqslant 4.0, \\ \frac{1}{2\pi}\sum_{l=0}^{1}\left(l+\frac{1}{2}\right)P_l(\mu)\exp[-l(l+1)s], & \text{for} \quad s > 4.0, \end{cases} \tag{5.1}$$

where $A(s)$ is the solution of Eq. (3.5).

Further optimization studies could be used to yield an optimal upper bound $m(s)$ for the sums in Eq. (5.1), and the following more general version may then be used:

$$f_a(\mu,s) = \begin{cases} \frac{A(s)}{4\pi \sinh A(s)} \exp[A(s)\mu], & \text{for} \quad s \leqslant s_0, \\ \frac{1}{2\pi}\sum_{l=0}^{m(s)}\left(l+\frac{1}{2}\right)P_l(\mu)\exp[-l(l+1)s], & \text{for} \quad s > s_0. \end{cases} \tag{5.2}$$

Given a numerical implementation of a result such as that of Eq. (5.1) or Eq. (5.2), on a mesh in the $(s,\mu) \in [0,\infty) \times [-1,1]$ plane one can compute the indefinite integral

$$F(\mu,s) = 2\pi \int_{-1}^{\mu} d\xi f(\xi,s),$$

the value of which lies between 0 and 1. Using Eq. (5.2) gives

$$F(\mu,s) = \begin{cases} \frac{1}{2\sinh A(s)}(\exp[A(s)\mu] - \exp[-A(s)]), & \text{for} \quad s \leqslant s_0, \\ \frac{1}{2}\sum_{l=0}^{m(s)}\{[P_{l+1}(\mu) - P_{l-1}(\mu)] - [P_{l+1}(-1) - P_{l-1}(-1)]\}\exp[-l(l+1)s], & \text{for} \quad s > s_0. \end{cases} \tag{5.3}$$

where the identity

$$\int_{-1}^{\mu} d\xi P_{l+1}(\xi) = \frac{1}{1+2l}([P_{l+1}(\mu) - P_{l-1}(\mu)] - [P_{l+1}(-1) - P_{l-1}(-1)])$$

has been used, with the convention $P_{-1}(\mu) = 0$. In the next step $F(\mu,s)$ is numerically inverted to obtain its inverse

$$F_I(F,s) \equiv F^{-1}(F,s) : [0,1] \times [0,\infty) \to [-1,1] \times [0,\infty)$$

on a mesh in the $(F,s) \in [0,1] \times [0,\infty)$ plane. F_I is the function needed for sampling the kernel using (pseudo)random numbers uniformly distributed in the interval [0,1]. The resulting table of values of $F_I(F,s)$ needs to be computed only once, given a choice of distribution of the (F,s) points on the mesh. A small preprocessor program or subroutine can be used to generate this table either as a file to be read in by the code that does the time advance, or as an initialization step in this code before the time advance is begun. In practice, it may be most expedient to compute and use the table directly only for intermediate values of s, $0.1 < s < 4.0$. For $s \leq 0.1$, an analytical inversion can be used exactly as for Nanbu's algorithm. For $s \geq 4.0$, a perturbative analytical calculation of the inversion can be used, based on the dominance of the first ($l = 0$) term in the sum in Eq. (5.3). Keeping only the $l = 0$ term in Eq. (5.3) gives the leading order solution

$$\mu(F,s) = F^I(F,s) \approx F - 1.$$

Inserting this into the remaining terms gives a more accurate approximation:

$$\mu(F,s) = F^I(F,s) \approx F - 1 - \frac{1}{2}\sum_{l=1}^{m(s)}\{[P_{l+1}(F-1) - P_{l-1}(F-1)] - [P_{l+1}(-1) - P_{l-1}(-1)]\}\exp[-l(l+1)s],$$

where only a small number of terms is needed.

Having computed and stored these values, the computation of collisions during the time advance in a simulation proceeds as follows. At any given time step, for each particle pair l with a s value s_l, use a standard pseudorandom number generator to generate a number r. Then, given this (r,s_l), use either interpolation (if $0.1 < s_l < 4.0$) or the analytical results for $F_l(F,s)$ (for $s_l \leq 0.1$ $s_l \geq 4.0$) to find an approximation to $F_l(r,s_l) = \mu$. This value of μ represents the cosine of the angle of the relative velocity vector of the pair with respect to the pre-collision direction.

For large time steps, the operator just described will produce a more accurate approximation to the Coulomb–Lorentz (or very small-mass-ratio interspecies scattering process) than Nanbu's original operator. The practical value of such an operator will depend on the situation in which it is used, because in applications the (Lorentz) pitch-angle scattering process takes place simultaneously with energy evolution due to scattering (if the mass ratio is not very small) or other processes (such as acceleration by collective or macroscopic electric or magnetic fields). An accurate representation of such processes may still require small frequent collisional time sub steps interspersed with sub steps that advance the effects of the other competing processes.

6. Conclusions

We have investigated the accuracy of and assumptions underlying Nanbu's collision operator [3]. It was argued that the numerical experiments that resulted in the parameterized collision kernel of [3] were (apart from statistical and finite time-stepping errors) numerical realizations of the Lorentz pitch-angle scattering process, for which an analytical solution for the collision kernel has long been known [1]. It was demonstrated empirically that, consistent with this argument, Nanbu's collision operator quite accurately recovers the effects of Coulomb–Lorentz pitch-angle collisions, or processes that approximate these (e.g., interspecies charged particle collisions with very small mass ratio) even for very large values of the collisional time step. Further, through an investigation of the analytical kernel, it was shown that Nanbu's parameterized kernel is highly accurate for small values of the normalized collision time step, but loses some of its accuracy for larger values of the time step. Careful numerical and analytical investigations were presented, which showed that the time dependence of the relaxation of a temperature anisotropy by Coulomb–Lorentz collisions has a richer structure than previously thought, and is not accurately represented by an exponential decay with a single decay rate. Finally, based on the results of our investigations of the analytical and Nanbu kernels, a practical collision algorithm was proposed that for Coulomb–Lorentz pitch-angle collision dominated processes improves on the accuracy of Nanbu's algorithm.

Acknowledgment

The work of Cohen and Dimits was performed under the auspices of the US Department of Energy by Lawrence Livermore National Laboratory under Contract DE-AC52-07NA27344. The work of Caflisch, Wang and Huang was supported in part by Grant DE-FG02-05ER25710 from the US Department of Energy. This work was supported by the Office of Advanced Scientific Computing Research, DOE Office of Science, initiative on Multiscale Mathematics and Optimization for Complex Systems.

Appendix A. Evaluation of the scattering angle variance versus the minimum deflection angle

The integral $\langle\theta_1^2\rangle = 8\int_0^1[\tan^{-1}(\theta_{\min}/2\eta)]^2\eta d\eta$ [3], which is used to relate the variance in Nanbu's experiments to the minimum collisional deflection angle, can be evaluated using

$$8\int_0^1[\tan^{-1}(\theta_{\min}/2\eta)]^2\eta d\eta = 2\theta_{\min}^2\int_{\theta_{\min}/2}^{\infty}[\tan^{-1}(y)]^2y^{-3}dy. \tag{A.1}$$

An accurate approximation to this for sufficiently small θ_{min} can be obtained using $\tan(y)\approx y$ for $y \ll 1$, so that

$$\langle\theta_1^2\rangle \approx 2\theta_{\min}^2\left\{\int_{\theta_{\min}/2}^{\varepsilon}y^{-1}dy + \int_{\varepsilon}^{\infty}[\tan^{-1}(y)]^2y^{-3}dy\right\} = 2\theta_{\min}^2\left\{\log(2\varepsilon/\theta_{\min}) + \int_{\varepsilon}^{\infty}[\tan^{-1}(y)]^2y^{-3}dy\right\},$$

where $\theta_{\min}/2 < \varepsilon \ll 1$. Setting $\varepsilon = 0.1$ gives

$$\langle\theta_1^2\rangle \approx 2\theta_{\min}^2\{\log(0.2/\theta_{\min}) + 2.57145\}, \tag{A.2}$$

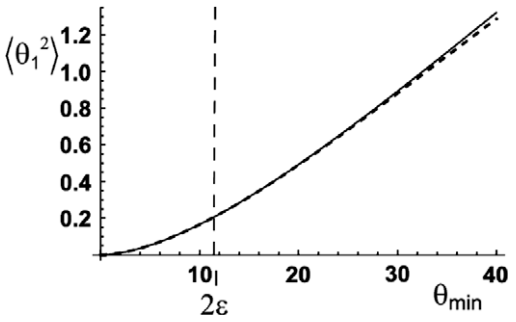

Fig. 13. $\langle\theta_1^2\rangle$ (in radians squared) vs. $\theta_{\min}$ (in degrees) from Eq. (A.2) (dashed curve) and from accurate direct numerical integration using Eq. (A.1).

Comparing this with a direct numerical evaluation gives excellent agreement up to $\theta_{min} \approx 30^\circ$ or 0.5 radians, as shown in Fig. 13. Shown also in this figure is the value (in degrees) used for 2ε, at which the logarithm term is zero.

Appendix B. Convolution of two Nanbu Kernels

Here, we evaluate the convolution of two Nanbu Kernels

$$N_2(\cdot, s_1, s_2) = N(\cdot, s_1) * N(\cdot, s_2),$$

where $N(\mu,s)$ is given by Eqs. (3.4) and (3.5). The simplicity of the Nanbu Kernel enables a straightforward evaluation of this convolution in closed form as a one-dimensional integral, which is easily evaluated numerically. Denote the two reference points and one integration point on the unit sphere, respectively as O, P and P', given by the unit vectors and polar coordinates $\hat{\mathbf{o}} : (\theta = 0), \hat{\mathbf{p}} : (\theta, \phi)$, and $\hat{\mathbf{p}}' : (\theta', \phi')$. Then

$$N_2(\mu, s_1, s_2) = \int dS_{P'} N(\mu', s_1) N(\hat{\mathbf{p}} \cdot \hat{\mathbf{p}}', s_2),$$

where $dS_{P'} = 2\pi d\mu' d\phi'$ is an area element for integration over points P' on the unit sphere, and $\mu' = cos\theta'$. Using

$$\hat{\mathbf{p}} \cdot \hat{\mathbf{p}}' = \sin\theta \sin\theta' \cos(\phi - \phi') + \cos\theta \cos\theta',$$

integrating over ϕ', and using $\oint d\phi' \exp(\alpha \cos\phi') = 2\pi I_0(\alpha)$, where I_0 denotes the modified Bessel function of order zero, gives

$$N_2(\mu, s_1, s_2) = 2\pi C(A_1) C(A_2) \int_{-1}^{1} d\mu' \exp[(A_1 + A_2\mu)\mu'] I_0\left(A_2 \sqrt{(1-\mu^2)(1-\mu'^2)}\right), \tag{B.1}$$

where

$$C(A_i) = \frac{A(s_i)}{4\pi \sinh A(s_i)}. \tag{B.2}$$

Eqs. (B.1) and (B.2) have been coded in Mathematica to yield the medium dashed curve in Fig. 11.

References

[1] B.A. Trubnikov, in: M.A. Leontovich (Ed.), Reviews of Plasma Physics, vol. 1, Consultants Bureau, New York, 1965, p. 105.
[2] T. Takizuka, H. Abe, J. Comp. Phys. 25 (1977) 205.
[3] K. Nanbu, Phys. Rev. E. 55 (1997) 4642–4652.
[4] R.J. Procassini, C.K. Birdsall, B.I. Cohen, Nucl. Fusion 30 (1990) 2329.
[5] R.J. Procassini, B.I. Cohen, J. Comp. Phys. 102 (1992) 39.
[6] P.W. Rambo, R.J. Procassini, Phys. Plasmas 2 (1995) 3130.
[7] P.W. Rambo, S.C. Wilks, W.L. Kruer, Phys. Rev. Lett. 79 (1997) 83.
[8] S. Ma, R.D. Sydora, J.M. Dawson, Comp. Phys. Commun. 77 (1993) 190–206.
[9] F. Taccogna, R. Schneider, K. Matyash, S. Longo, M. Capitelli, D. Tskhakaya, Contrib. Plasma Phys. 48 (2008) 147–152.
[10] C.M. Wang, T. Lin, R. Caflisch, B.I. Cohen, A.M. Dimits, J. Comp. Phys. 227 (2008) 4308.
[11] R. Caflisch, C.M. Wang, G. Dimarco, B. Cohen, A. Dimits, Multiscale modeling and simulation (SIAM) 7 (2008) 865–887.
[12] V.I. Kogan, Plasma Physics and the Problem of Controlled Thermonuclear Reactions, vol. 1, Pergamon Press, New York, 1961, p. 153.
[13] A.J.C. Ladd, W.G. Hoover, J. Stat. Phys. 38 (1985).
[14] F.D. Hinton, R.D. Hazeltine, Rev. Mod. Phys. 48 (1976).
[15] C.K. Li, R.D. Petrasso, Phys. Plasmas 13 (2006) 056314.
[16] A.V. Bobylev, K. Nanbu, Phys. Rev. E61 (2000) 4576–4582.
[17] H. Huba, NRL Plasma Formulary (2007, Naval Research Laboratory document: NRL/PU/6790-07-500, <http://wwwppd.nrl.navy.mil/nrlformulary/>, p. 33.